Published in final edited form as:
Mol Cancer Ther. 2009 August ; 8(8): 2183–2192. doi:10.1158/1535-7163.MCT-08-1203.

Three-Kinase Inhibitor Combination Recreates Multi-Pathway Effects of a Geldanamycin Analog on Hepatocellular Carcinoma Cell Death

Justin R. Pritchard[1], **Benjamin D. Cosgrove**[2], **Michael T. Hemann**[1], **Linda G. Griffith**[2], **Jack R. Wands**[3], and **Douglas A. Lauffenburger**[1,2]

[1]Department of Biology, Massachusetts Institute of Technology, Cambridge, MA

[2]Department of Biological Engineering, Massachusetts Institute of Technology Cambridge, MA

[3]The Warren Alpert Medical School of Brown University. Providence, RI

Abstract

Multi-target compounds that act on a diverse set of regulatory pathways are emerging as a therapeutic approach for a variety of cancers. Toward a more specified use of this approach, we hypothesize that the desired efficacy can be recreated in terms of a particular combination of relatively more specific (i.e., ostensibly single-target) compounds. We test this hypothesis for the geldanamycin analog 17AAG in hepatocellular carcinoma (HCC) cells, measuring critical phosphorylation levels that indicate the kinase pathway effects correlating with apoptotic responsiveness of the Hep3B cell line in contrast to the apoptotic resistance of the Huh7 cell line. A principal components analysis constructed from time-course measurements of 7 phospho-protein signaling levels identified modulation of the AKT, IKK and STAT3 pathways by 17AAG treatment as most important for distinguishing these cell-specific death responses. The analysis correctly suggested from 17AAG-induced effects on these phospho-protein levels that the FOCUS cell line would show apoptotic responsiveness similarly to Hep3B. The PCA also guided the inhibition of three critical pathways and rendered Huh7 cells responsive to 17AAG. Strikingly, in all three HCC lines the three-inhibitor combination alone exhibited similar or greater efficacy to 17AAG. We conclude that: (a) the principal components analysis captures and clusters the multi-pathway phospho-protein timecourses with respect to their 17AAG-induced apoptotic responsiveness;...(passage deleted)... (b) we can recreate, in a more specified manner, the cellular responses of a prospective multi-target cancer therapeutic.

Keywords

17AAG; apoptosis; signaling; computational modeling

Introduction

The fairly limited success of many targeted cancer therapeutics when used as single-agent treatments presents a challenging problem that has motivated studies seeking to: stratify failure-vs-success categories (1) or to combine targeted therapeutics with traditional chemotherapeutic regimes (2). An alternative avenue generating growing interest is a new class of compounds

Author Correspondence Douglas Lauffenburger, M.I.T. Department of Biological Engineering, 77 Massachusetts Ave., Cambridge MA 02139; lauffen@mit.edu.

Conflict of Interest
The authors report no conflicts of interest

known as multi-target drugs (3). These compounds aim to improve therapeutic efficacy by producing a combined inhibition of diverse regulatory pathways that are important for cancer cell proliferation and survival.

At one end of the multi-target drug spectrum lies a class of Hsp90 inhibitors such as 17AAG, which were derived from the tumoricidal natural product Geldanamycin (4). Hsp90 is a vital chaperone that, relative to other chaperones, interacts with a select but critical subset of cellular proteins including nuclear hormone receptors and components of signal transduction cascades (5). Hsp90 inhibition appears to offer a promising anti-cancer strategy (6) but, compared to more traditional targeted therapeutics, an exceptionally pleiotropic effect. In a recent genome-wide study in *Saccharomyces cerevisiae*, Hsp90 was found to interact with roughly 10% of the ORFs investigated (7).

The nature of the effects of 17AAG in tumor cells relative to non-transformed cells appears to derive from the enhanced binding of 17AAG to Hsp90 in the former. Tumor cell Hsp90 is found more highly resident in multi-chaperone complexes with high rates of ATPase activity, constituting a distinctive molecular state exhibiting an approximately 10-fold greater binding affinity for 17AAG compared to that in the normal cells (8). Hsp90 inhibition in a variety of tumor cell lines has been shown to affect the levels and/or activity of ErbB family receptors, Src, Ras, Raf, AKT, IKK, Janus kinase, Her2, p53, RIP, and cell cycle regulators, as well as increasing the levels of the anti-apoptotic chaperone Hsp70 (5,9–14). In addition to these long-term effects on client protein levels and their associated downstream signaling effects, short-term effects of Hsp90 inhibitors have also been observed. Geldanamycin treatment has been found to yield increased phosphorylation of AKT in myocytes (15), increased PKR activity and phosphorylation of eIF-2α in HeLa cells (16), and transient early signaling in the Src, AKT, and ERK pathways in both MCF-7 and COS7 cells (17). However, the contributions of these various pathways effects to cell death responses are unclear, and the manner by which these effects integrate to impact cell behavior is even more difficult to ascertain.

Our goal is to offer an effective approach based upon systematically extracting the critical effects of multi-target compounds, which could enable the rationale recreation of their effectiveness via designed combinations of more selectively targeted drugs. Since Hsp90 inhibition elicits contradictory effects: the degradation of proteins involved in cellular survival, as well as an increase in HSP70 levels, we reason that a rational recreation of its pro-apoptotic effects may potentially increase efficacy. Our approach is motivated by recent successes in computational characterization of the effects of diverse drug induced perturbations governing cellular phenotypes (18,19). Data-driven computational modeling techniques such as principal components analysis (PCA) and partial least-square regression (PLSR) seek to find key vectors representing signal combinations that contain the most vital information for predicting – at least in correlative fashion – cell responses to various stimuli (19).

We test this hypothesis on quantitative experimental measurement of multiple phosphoprotein signaling pathways altered by 17AAG in a set of HCC cell lines. A principal components analysis of time-course data for 7 kinase signals reveals that early effects of 17AAG on the AKT, IKK and STAT3 pathways are predominantly critical for clustering cell-specific apoptotic death responses among the Hep3B, Huh7, and FOCUS lines. While individual inhibition of each of these three pathways had little effect on the cell responses, combining all three kinase inhibitors rendered the 17AAG-resistant Huh7 line responsive and had greater efficacy than 17AAG itself in two of our three cell lines.

Materials and Methods

Cell Lines and Culture

Hep3B, Huh7 and FOCUS cell lines (20) were obtained from the Wands Lab (Brown University, Providence RI). Cells were maintained in Minimal Essential Media (ATCC Manassas VA) with 10% FBS (HyClone, Omaha NE) at sub-confluent densities and 37°C, 5% CO_2. Apoptosis and signaling experiments were seeded at cell densities of 200,000, and 150,000 cells per well of a 6-well plate for Hep3B and Huh7/Focus cell lines respectively. (section deleted)

Inhibitors

All inhibitors were purchased from Calbiochem (San Diego, CA). 17AAG (cat# 100068) was reconstituted in methanol; all other compounds (BMS-345541 cat# 401480, JAK inhibitor 1, Pyridone 6 cat# 420099, PI103 cat# 528100,) were reconstituted in DMSO. PD98059 (Calbiochem cat #513000) reconstituted in DMSO is the MEK inhibitor used in the control combination study (Figure S2), and the JNK inhibitor is SP600125 (Calbiochem cat#420119). (section deleted)

Signaling Measurements

Signaling measurements were made using bead based ELISA kits manufactured by Bio-Rad. Bioplex assays were run according to all of the manufacture's recommendations. These Bioplex assays were used to measure p-AKT (Ser473), p-ERK1/2 (Thr202/Tyr204), p-STAT-3 (Tyr705), p-p38 (Thr180/Tyr182), p-JNK (Thr183/Tyr185), p-GSK-3α/β (Ser21/Ser9), p-IKb-α (Ser32), AKT, p38, and ERK. All measurements are the mean of duplicates. Measurements were taken at 0, 1, 2, 4, and 24 hours after addition of 1 μM 17AAG, and were normalized to unstimulated controls on a cell line by cell line basis. This fold-change normalization created a relative value of 1 for all signals in all cell lines at the point of 17AAG addition. This allowed direct comparison of the fold change of 17AAG effects across cell lines.

Apoptosis Assays

Cells were harvested from 6 well plates and combined with the floating fraction. This sample was fixed in 3–4% Para-Formaldehyde, then permeabilized for antibody staining in methanol and stored at −20° C for up to 1 week. Cells were stained with antibodies for Cleaved (Activated) Caspase 3 (BD Pharmingen, San Jose, CA, cat# 559565) and Cleaved PARP (BD Pharmingen cat# 51–9000017) at a dilution of 1:300 (in PBS-0.1%Tween20–1%BSA). Secondary antibodies were IgG Alexa Flour 647 and Alexa Fluor 488 (Invitrogen cat # A21245 and A11029 respectively) at 1:300 in PBS-TB. A minimum 10,000 gated events were collected per sample. All measurements are the mean of triplicates +/- SEM.

Data Analysis

Principal Components Analysis (PCA) (21) was done using Simca-p++ v11.5 (22). All signals were mean centered and unit variance scaled before analysis. This centering and scaling allows all signaling variables to be considered on an equal scale in principal components space, based solely upon induced variation relative to the mean of a given signal and its position in the distribution. Principal Components Analysis finds directions of covariance in the original data set. These directions become the principal components onto which the original data set is collapsed. Our initial multi-dimensional data is condensed down into 2 principal components dimensions that capture the majority of the variance. Loadings plots are created by plotting the original time dimension in the 2 component graph. Scores plot are generated by plotting the original signaling data in the two component plot. Hotelling's criterion displays the distance in the model plane at which a given sample is behaving significantly different than the rest of

the data with 95% confidence (23). For an intuitive description of PCA see Supplementary Figure 1. In our dataset, we use a variation of Principle Components cluster analysis. Since all of our signaling variables cannot be segmented into completely separable groups, we use a "dissection" or "segmentation" based technique (21). Here we calculate a Euclidean distance based upon the original variables (a contributions vector) to identify signals that are the most distinct between sensitive and resistant cell lines.

The appropriate threshold to interpret the PCA was decided upon by the small increase in goodness of fit that was provided by a third component. To determine whether or not the percentage of the cumulative variance explained by our model was significant, we generated 1000 data matrices of the same size as our original dataset. The data matrix entries were found by randomly sampling the column indices across a signaling row. This perturbation retains similar variance structure to the original signal. Our test statistic was the cumulative percentage of the variance explained by a 2 component model built in Matlabv7.0 (using the princomp.m function) on these 1000 data matrices. The test statistic was then plotted as a histogram, a normal distribution was fit to the data, and a p-value was calculated using the Cumulative Distribution Function (CDF).

0–4hr integrals were calculated using a 2^{nd} order polynomial curve fit followed by numerical integration using a 0.2 hr increment. Heat maps were made in Matlabv7.0. The analysis of synergy was coded using Matlab. Statistical comparisons of cell death were done using a Student's t-test. P-values <0.05 were deemed significant.

Results

Conventional markers of 17AAG action cannot account for the differential cell death responses in Huh7 and Hep3B cells

The effect of 17AAG treatment on cell death in hepatocellular carcinoma cell lines was assessed by treating Huh7 and Hep3B with 17AAG at 0.1 and 1μM for 48 hours. A representative gating for a population staining double positive for active (cleaved) Caspase 3 and cleaved PARP was assessed via flow cytometry (Figure 1A). Double positive cells represent the population of cells within a well that are undergoing apoptosis. The same gating thresholds were used for all of the samples from a given cell line and are based upon the negative control. No single positive populations were noted at 48 hours during the duration of our study. 3 samples per cell line/condition were averaged using the values obtained from the plots in 1A and are plotted in Figure 1B. Hep3B cells were found to be sensitive to 1μM 17AAG induced cell death, whereas Huh7 cells were found to be resistant (Figure 1B). We then hypothesized that a difference in the levels of p-AKT (S473), t-AKT, p-ERK1/2(T202, Y204), and p-IκB-α (S32/S36) 24 hours after the addition of 17AAG might account for the difference in phenotype (Figure 1C). Lysates were collected both before and 24 hours after treatment with 17AAG. The relative decrease in these 4 measurements at 24 hours is identical in sensitive and resistant cell lines. These late-time measurements indicate that a simple explanation regarding the long-term signaling degradation arising from 17AAG treatment is not able to explain the disparate death responses of Hep3B and Huh7 cells.

A dynamic multi-pathway analysis can distinguish Huh7 resistance and Hep3B sensitivity to 17AAG

Since the degradation of PI3K–AKT, Ras/Raf/Mek/ERK, and IKK-NF-κB pathway signaling at 24 hours failed to distinguish Huh7 from Hep3B, we proposed that a dynamic study including measurements of the shorter-term effects of 17AAG treatment might yield information that could distinguish the differential response behaviors of these cell lines. We thus measured the levels of the same signals at 0, 1, 2, 4, and 24 hours after treatment in both the Huh7 and Hep3B

cells. These timepoints were initially chosen based upon the literature reports of early and late changes in phosphorylation levels in response to 17AAG (17). These measurements were normalized to an un-treated control for each cell line, and are plotted in Figure 2A as fold-change induced by 17AAG. Both Huh7 and Hep3B exhibited transient early p-JNK activation. However, relatively stronger transient activation and/or relatively weaker degradation was seen for most other signals (p-AKT, p-IκB-α, p-GSK3α/β, p-ERK1/2, p-p38 and p-STAT3) in Huh7 cells compared to Hep3B cells (Figure 2A). Strikingly, the integrated signal changes over the first 4 hours after 17AAG treatment are higher across many components in Huh7 cells than in Hep3B cells (Figure 2B). In order to more effectively interpret these data we employed principal components analysis, a technique that models multi-variate data in terms of key combinations of measurements exhibiting major co-variation in the data set. These combinations can be viewed geometrically as “directions” (or vectors) in the “space” of the signaling measurements defined by axes representing a combination of the measured time-points and the integral metric. The direction of greatest co-variation (an axis representing the timepoints that are most similar), incorporates the most important measurement combinations, is the principal component #1 (PC1); principal component #2 (PC2) then incorporates the next most important measurement combinations best capturing the residual co-variation, and so on. The principal components taken all together collapse the original multi dimensional data into a reduced number of axes representing the most important underlying variables. In our case viewing a “loadings plot”,(data summarized in figure 3C), the 6 dimensional data set(1hr,2hr, 4hr, 24hr and Early/Late integral metrics) can be comprehended in 2 dimensional principal components space as early signaling(representing primarily 1hr, 2hr, and the early integral data) (PC1) and late signaling(where the 24hr data projects most strongly) (PC2). These underlying variables are just combinations of the original variables that best comprehend the data within the entire signaling measurement ‘vector space’ (Supplementary Figure S1 offers an illustrative tutorial). Our model with 2 principal components effectively captures 91% of the cumulative variance. Our cutoff was readily established by the major drop in the variance captured by the third component (Figure 3A). Furthermore a re-sampling of our data set determined that our analysis captures significantly($p=0.0002$) greater variance than one can capture with 1000 2-component models generated by randomly sampling the column index of the rows in our data set(Figure 3B). Our analysis visually distinguishes the behavior of both Huh7 and Hep3B cells. A so-called ‘scores plot’, in which the various signaling measurements are projected on the principal components axes, visualizes distinct regions where Huh7 signals reside differentially with respect to Hep3B signals (Figure 3C). These differences are quantified in Figure 2D, in terms of ‘contribution vectors’, which quantify the disparities between cell line-specific signals (in units of standard deviation) relative to the average distance between all of the signals of the distinct cell lines. The calculated contributions vectors reveal that out of the 10 signaling measurements made at each of 5 time-points, the most important differences between the drug resistant Huh7 and drug sensitive Hep3B lie in the early time-points of four signals: p-AKT, p-IκB-α, p-STAT3, and p-p38. Because the experimental conditions for the elucidation of the signaling effects grows very rapidly with the size of the hit set, the p-p38 signaling measurements were excluded from further analysis since they reside as an outlier beyond the region of Hotelling’s criterion (23), and presented no clear biological hypothesis.

The principal components model accurately maps another 17AAG-sensitive HCC cell line, FOCUS, to the same region as Hep3B

In order to test our principal components analysis we utilized our previous approach in a third HCC cell line. A signaling time-course for FOCUS cells, analogous to Figure 2A, shows signal degradation and no transient activation (Figure 4B). Although certain signaling network differences between FOCUS and Hep3B signaling are evident by inspection, our principal components analysis shows that the FOCUS cells cluster in the same region as the similarly

17AAG sensitive Hep3B cells (Figure 4C). Indeed, we found that FOCUS cells are sensitive to 1μM 17AAG-induced cell death at 48 hours (Figure 4A). This result demonstrates that the principal components capture critical signal combinations associated with these cell death-vs-survival outcomes.

A drug combination pretreatment based on inhibition of three key nodes partially sensitizes Huh7 to 17AAG

In Figure 3D we identified four signals (p-AKT, p- IκB-α, p-STAT3, and p-p38) to be most important in distinguishing Huh7 from Hep3B. We proposed to test whether a combination of drugs inhibiting these key signals in particular could recreate the 17AAG treatment responses. We selected p-AKT, p-STAT3, and p- IκB-α for this purpose, omitting p-p38 due to its notification by Hotelling's outlier criteria at a 95% confidence level (23). Pre-treatment of Huh7 cells for 12 hours with targeted inhibitors of p-AKT (PI3Kinhibitor, PI-103, 5μM), p-STAT3 (JAK inhibitor 1, Pyridone 6,Calbiochem, 3μM) and p-IκB-α (IKK inhibitor, BMS-345541, 15μM) signaling failed to sensitize Huh7 cells to 1μM 17AAG at 48hours (Figure 5A). However, a combination pre-treatment using all three inhibitors together partially sensitized ($p<0.0001$) Huh7 cells to 17AAG-induced cell death (Figure 5A). Moreover, this inhibitor combination induced Huh7 cell death to a significantly greater ($p<0.0005$) degree than did 17AAG (Figure 5A). In order to control for the possibility that any combination of three inhibitors can potentiate 17AAG induced cell death, inhibition of one critical signal (p-STAT3) was combined with inhibition of two non-critical signals (p-JNK, p–ERK) (Figure 3D). This control drug combination, comprising 3μM of the JAK inhibitor, 10μM of a MEK inhibitor (PD98059) and 10μM of a JNK inhibitor (SP600125), failed to sensitize Huh7 to 17AAG or induce cell death on its own at 48 hours. (Figure S2).

Decoupling pro-apoptotic effects from the overall context of 17AAG treatment creates a three-kinase inhibitor combination that works as well or better than 17AAG in all cell lines

17AAG is known to have both pro and anti apoptotic effects. Assuming that 17AAG induces cell death through a combination of the pro-apoptotic consequences of the degradation of key signaling pathway nodes, we hypothesized that the previously identified critical nodes distinguishing sensitive and resistant cells could be key sites for selectively-targeted drug contributions in sensitive cells. To test this idea, FOCUS and Hep3B cells were pre-treated with the three-kinase drug combination, or control vehicle, for 12 hours before addition of 1μM 17AAG. The drug combination enhanced 17AAG induced cell death significantly ($p=0.050$, and $p<0.0001$ respectively) in both cases (Figure 5B). Yet more strikingly, the drug combination by itself induced cell death as strongly -- or more so -- than 17AAG in all HCC cell lines. FOCUS cells showed no significant difference between 17AAG and the drug combination induced cell death, whereas in Hep3B and Huh7 cells the drug combination at 48 hours worked significantly better than 17AAG (Figure 5A, B).

Decoupling the pro-apoptotic effects from their 17AAG context allows for cell line specific tuning of the therapeutic strategy

After finding a drug combination that works as well or better than 17AAG, we wanted to test two hypotheses. First, that the decoupling of a specific pathway effect from the context of 17AAG allows for cell line specific therapeutic strategies. And, second, that the presence of additivity or synergy correlates with cell line-specific differences in the combination inhibitor efficacy relative to 17AAG. To address these questions, we undertook a set of experiments in a Jak inhibitor background, across a 4×4 matrix of PI3K and IKK inhibitor concentration combinations, covering 4 concentrations of each (0, Low, Medium, and High) (Figure 6). Inspection of the cell death responses reported in this matrix indicated distinct responses for the three cell lines tested. FOCUS cells appeared to primarily be sensitive to the IKK inhibitor

in the JAK inhibitor background whereas Hep3B and Huh7 cells exhibited sensitivity to both IKK and PI3K inhibition (Figure 6A). Calculation of the fold increase in cell death of a double drugged entry in the 4×4 dosing matrix relative to linear additivity demonstrates that only Huh7 cells exhibit a drug combination synergy (Figure 6B). This finding of multi-drug nonlinear synergy in the Huh7 and multi-drug additivity in Hep3B but not FOCUS cells correlates with our observation that the kinase inhibitor combination could essentially duplicate the 17AAG effects on cell death in the latter whereas it could exceed the 17AAG effects on cell death in the former 2.

Discussion

Inhibition of the Hsp90 chaperone represents a prominent example of a highly complex multi-target therapeutic approach to cancer (5), and studies have explored the myriad of regulatory pathway alterations associated with its effects (5,9–17). Although these studies have unveiled short-term and/or long-term changes in levels and/or activities of numerous cellular components with opposing effects on the downstream phenotype, there is currently inadequate understanding which set of pathway alterations can recapitulate drug efficacy. Our effort here aims to gain quantitative understanding of the key kinase signals underlying the effects of the geldanamycin analogue 17AAG on differential apoptotic death responses of three HCC cell lines: Hep3B, FOCUS, and Huh7. Our studies centered on 7 canonical kinase signaling effects: p-AKT (Ser473), p-ERK1/2 (Thr202/Tyr204), p-STAT-3 (Tyr705), p-p38 (Thr180/Tyr182), p-JNK (Thr183/Tyr185), p-GSK-3α/β (Ser21/Ser9), and p-IKb-α (Ser32), with a goal of ascertaining whether a quantitative combination of a particular subset of these signals might be especially critical in clustering the HCC line responses to 17AAG. (passage deleted)

We found that a PCA-based model consisting of 2 principal components explains 91% of the cumulative variance captured by the model. This variation can be classified as early variation (PC1) and late variation (PC2) (Figure 3). All cell lines and signals inhabit the same principal components space, implying that there is a general homology of response. This overall homology stresses that the drug is operating similarly in all cell lines tested, and that the phenotypic responses are not likely to be based upon the metabolic inactivation of 17AAG or a rapid cellular efflux. The early variation axis (PC1) best separates the cell lines with disparate responses, suggesting, that this previously documented early signaling phenomena (17) can be correlated with a cellular phenotype.

The PCA based visualization accurately maps the sensitive FOCUS cell line to the same region as Hep3B cells (Figure 4). This greatly improves our confidence that the variation captured in 2 dimensional principal components space is relevant to the disparate cell phenotypes, and that our analysis has captured important biological information. The success of our PCA mappings suggests that data-driven modeling can effectively reduce the dimensionality of multi-target perturbations, and provide a compact easy to interpret analytical method for determining the most phenotypically relevant parameters for further investigations.

Previous data-driven modeling efforts (24,25), have shown that a systematic signaling analysis of growth factor and cytokine induced cellular phenotypes, captures enough signaling variation that the phenotypic effects of drug perturbations can be predicted *a priori*. Kumar et al. (18) extended this analysis to show that multiple signals measuring the off target effects of inhibitors are necessary to predict drug effects upon EGF-induced migration. Our quantitative analysis of 17AAG leads to testable hypotheses about the targeting of early IKK, PI3K, JAK-STAT inhibition in 17AAG induced cell death (Figure 2). The individual targeted pharmacological pre-treatment of these three survival pathways, fails to abrogate the resistance phenotype, but the combined pretreatment is able to synergistically sensitize Huh7 to 17AAG (Figure 5A).

This evidence suggests that cumulative early action of the IKK, PI3K, and JAK-STAT pathway families may be responsible for a portion of Huh7's drug resistance phenotype.

While the combination therapy potentiates 17AAG induced cell death in all cell lines tested, the most striking consequence of our study, is the ability of combination therapy alone to recapitulate 17AAG's cell death effect in a manner that is equal to, or greater than the singular effect of 17AAG. This effect has two distinct modalities. In Huh7 and Hep3B cells the combination treatment works approximately 5-fold and 3-fold better, respectively, than 17AAG alone. In contrast, the combination treatment is of similar efficacy to 17AAG alone in FOCUS cells (Figure 5). These distinct modalities can be correlated with the spectrum of multiple drug interactions in the combination therapy (Figure 6). We speculate that these correlations may suggest a basis for future work on the cell specific nature of both 17AAG's pro-/anti-apoptotic function, and how synergy between nodes may play a role in the efficacy of multi-drug combinations and multi-target inhibitors.

By using principal components modeling of a drug perturbation to guide the recreation of a more specific therapeutic strategy we have shown that we can not only recreate the effect of a multi-target drug, but that the recreated effect can work better than the original drug. The existence of differences in the multi-drug interactions (Figure 6) underscores the value of recreating multi-target effects. In decoupling the effects from the context of 17AAG we find that the potential exists to allow for the individual adjustment of the elements of a combination therapy.

Our suggestion that a specified combination therapy may produce a less generally pleiotropic effect than the multi-target compound from which it has been rebuilt arises from comparative consideration of the diversity of the cellular effects of the initial multi-target compound along with the off-target effects of the combination therapy. In our particular case, which is certainly a fairly extreme example, Hsp90 in *Saccharomyces Cerevisiae* is known to interact with approximately 10% of the ORFs examined in a recent study (Zhao et al., 2005). Although a similar analysis is not available for the three compounds of our combination therapy, it seems plausible that our combination therapy is less broadly cross-reactive for several reasons. A systematic study of 317 kinases found that for PI103, approximately 10 cellular kinases had IC50's of less than 10μM in vitro (26) BMS-345541 is an allosteric inhibitor of IKK and failed to significantly inhibit a panel of 15 related kinases at concentrations as high as 100μM (27). Our Janus kinase inhibitor, Pyridone 6, while less well tested than the other two fails to inhibit the proliferation of cell lines that do not harbor activated JAK-STAT signaling (28). Thus in-spite of the inevitable existence of some off-target effects, it seems highly unlikely that the magnitude of these effects could approach the pleiotropy of 17AAG. Therefore, the generalizability of this approach to other forms of multi-target compounds will likely prove increasingly practical as more specific inhibitors become available.

Supplementary Material

Refer to Web version on PubMed Central for supplementary material.

Acknowledgments

The authors would like to thank Hyung-Do Kim, and Luke Gilbert for insightful discussions, and Pam Kreeger, Megan Palmer, Shannon Alford, Shan Wu, Matt Lazzara, and Arthur Goldsipe for excellent technical input.

Financial support: This work was funded in part by an NIH training grant to the MIT Biology Department, an MIT Presidential Fellowship to J.R.P., the NCI Integrative Cancer Biology Program, and the NIGMS Cell Decision Processes Center.

References

1. Lynch TJ, Bell DW, Sordella R, et al. Activating mutations in the epidermal growth factor receptor underlying responsiveness of non-small-cell lung cancer to Eng gefitinib. New J Med 2004;350:2129–2139.
2. Chabner BA, Roberts TG Jr. Chemotherapy and the war on cancer. Nat. Rev. Cancer 2005;5:65–71. [PubMed: 15630416]
3. Petrelli A, Giordano S. From single to multi-target drugs in cancer therapy: when aspecificty becomes an advantage. Curr. Med. Chem 2008;15:422–432. [PubMed: 18288997]
4. Uehara Y, Makoto H, Tomio T, Umezawa H. Phenotypic change from transformed to normal induced by benzoquinonoid ansamycins accompanies inactivation of p60src in rat kidney cells infected with Rous sarcoma virus. Molecular Cell. Biol 1986;6:2198–2206.
5. Whitesell L, Lindquist S. Hsp90 and the chaperoning of cancer. Nat. Rev. Cancer 2005;5:761–772. [PubMed: 16175177]
6. Whitesell L, Shifrin SD, Schwab G, Neckers L. Benzoquinonoid ansamycins possess selective tumoricidal activity unrelated to src kinase inhibition. Cancer Res 1992;52:1721–1728. [PubMed: 1551101]
7. Zhao R, Davey M, Hsu YC, et al. Navigating the chaperone network: an integrative map of physical and genetic interactions mediated by the Hsp90 chaperone. Cell 2005;120:715–727. [PubMed: 15766533]
8. Kamal A, Thao L, Sensintaffar J, et al. A high-affinity conformation of Hsp90 confers tumour selectivity on Hsp90 inhibitors. Nature 2003;425:407–410. [PubMed: 14508491]
9. Hostein I, Robertson D, DiStefano F, et al. Inhibition of signal transduction by the Hsp90 inhibitor 17-Allyamino-17-demethoxygeldanamycin results in cytostasis and apoptosis. Cancer Res 2001;61:4003–4009. [PubMed: 11358818]
10. Bareng J, Jilani I, Gorre M, et al. A potential role for Hsp90 inhibitors in the treatment of Jak2 mutant-positive diseases as demonstrated using quantitative flow cytometry. Leukemia and Lymphoma 2007;48:2189–2195. [PubMed: 17926180]
11. Mitsiades CS, Mitsiades NS, McMullan CJ, et al. Antimyeloma activity of heat shock protein-90 inhibition. Blood 2006;107:1092–1100. [PubMed: 16234364]
12. Garcia-Morales P, Carrasco-Garcia E, Ruiz-Rico P, et al. Inhibition of Hsp90 function by ansamycins causes downregulation of cdc2 and cdc25c and G2/M arrest in glioblastoma cell lines. Oncogene 2007;26:7185–7193. [PubMed: 17525741]
13. Solit DB, Ivy SP, Kopli C. Phase 1 trial of 17-Allyamino-17-demethoxygeldanamycin in patients with advanced cancer. Clin. Cancer Res 2007;13:1775–1782. [PubMed: 17363532]
14. Chandarlapaty S, Sawai A, Qing Y, et al. Snx2112 a synthetic heat shock protein 90 inhibitor has potent antitumor activity against HER kinase-dependent cancers. Clin Cancer Res 2008;14:240–248. [PubMed: 18172276]
15. Yun BG, Matts R. Hsp90 functions to balance the phosphorylation state of Akt during C2C12 myoblast differentiation. Cellular Signaling 2005;17:1477–1485.
16. Donze O, Abbas-Terki T, Picard D. The Hsp90 chaperone is both a facilitator and a repressor of the dsRNA-dependent kinase PKR. The EMBO J 2001;20:3771–3780.
17. Koga F, Xu W, Karpova TS, et al. Hsp90 inhibition transiently activates Src and promotes Src-dependent Akt and Erk activation. PNAS 2006;103:11318–11322. [PubMed: 16844778]
18. Kumar N, Afeyan R, Kim HD, Lauffenburger DA. A multi-pathway model enables prediction of kinase inhibitor cross-talk effects on migration of Her2-overexpressing mammary epithelial cells. Mol Pharmacol 2008;73:1668–1678. [PubMed: 18349105]
19. Janes KA, Yaffe MB. Data-driven modeling of signal-transduction networks. Nat. Rev. Mol. Cell Biol 2006;7:820–828. [PubMed: 17057752]
21. Jolliffe, IT. Vol. 2nd Edition.. New York: Springer-Verlag; 2002. Principal Components Analysis.
22. Eriksson, L.; Johansson, E.; Kettanel, N.; Wold, S. Sweden: UMETRICS A.B. Umea; Multi and Mega-variate Data Analysis, Principles and Applications.
23. Mardia, KV.; Kent, JT.; Bibby, JM. Multivariate Analysis. Academic Press; 1979.

24. Miller-Jensen K, Janes KA, Brugge JS, Lauffenburger DA. Common effector processing mediates cell-specific responses to stimuli. Nature 2007;448:604–608. [PubMed: 17637676]

25. Kemp ML, Wille L, Lewis CL, Nicholson LB, Lauffenburger DA. Quantitative network signal combinations downstream of TCR activation can predict IL-2 production response. J Immunol 2007;178:4984–4992. [PubMed: 17404280]

26. Karaman MW, Herrgard S, Treiber DK, et al. A quantitative analysis of kinase inhibitor selectivity. Nat. Biotechnol 2008;26:127–132. [PubMed: 18183025]

27. Karin M, Yamamoto Y, Wang QM. The IKK NF-KB system: a treasure trove for drug development. Nat. Rev. Drug Disc 2004;3:17–26.

28. Pedranzini L, Dechow T, Berishaj M, et al. Pyridone 6, A pan-Janus-Activated Kinase inhibitor induces growth inhibition of multiple myeloma cells. Cancer Res 2006;66:9714–9721. [PubMed: 17018630]

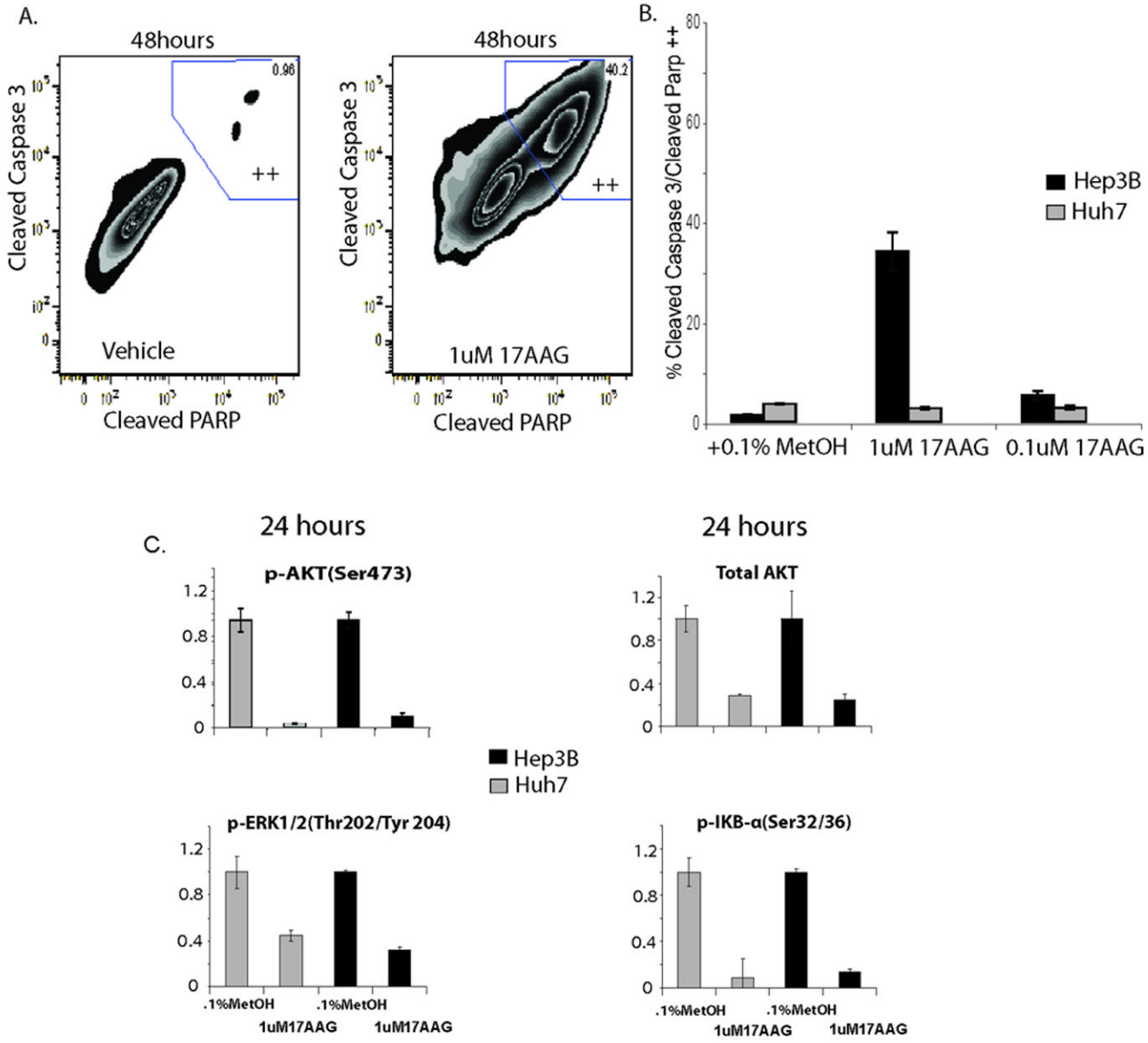

Figure 1.

A plot for the Cleaved Caspase 3/Cleaved PARP double positive population at 48 hours measures the susceptibility of Hep3B and the resistance of Huh7 cells to 17AAG. Typical measurements of 24hr signaling degradation in response to 17AAG fail to correlate with this distinction. **A** A representative flow cytometry scatter plot depicts Hep3B fixed and permeabilized cells, that are stained with antibodies for Active Cleaved Caspase 3 and Cleaved PARP at 48hrs after treatment with 1μM17AAG or 0.1% MetOH vehicle control. The double positive population is denoted by the gating in the upper right hand corner. Different gatings were used for Huh7 and Hep3B but the scatter plots looked very similar. **B** The average size of the population of three replicates(+/−SEM) of Hep3B and Huh7 cells as gated in A. represents the percent of double positive apoptotic cells at 48hrs +/−SEM. **C** Late time signals do not correlate with 17AAG susceptibility. Measured at 24hours, the fold change of the mean of duplicates +/−SEM, treated with 1uM 17AAG, is normalized to a 0.1% MetOH control. p-

AKT (Ser473), t-AKT, p-ERK1/2(Thr202/Tyr204), and p-IKB-α (Ser32/36) were measured by a bead based Bio-rad phospho-protein (Bioplex) assay.

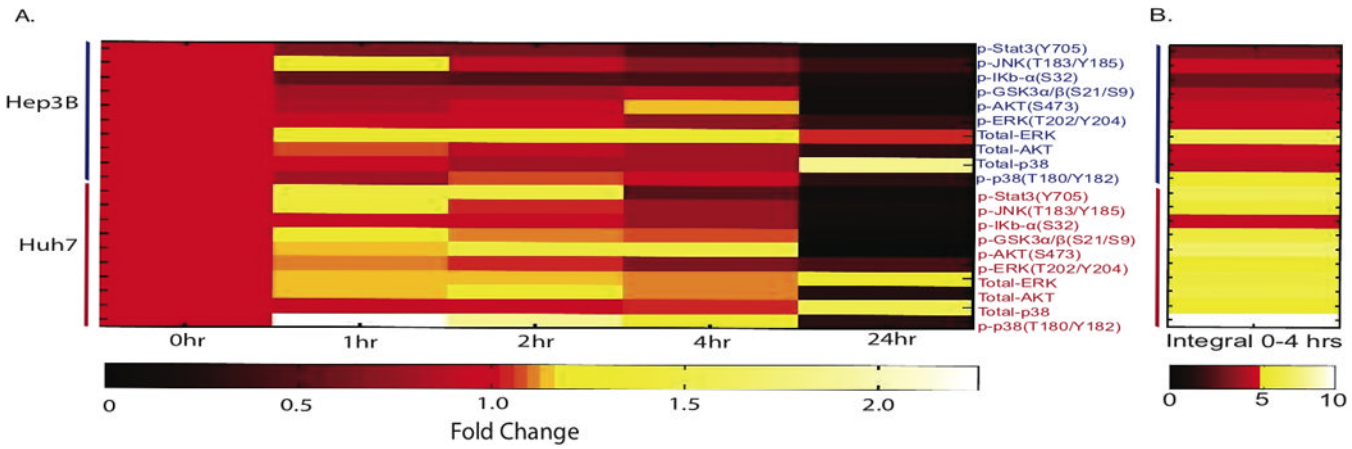

Figure 2.

A dynamic signaling timecourse reveals differences between Hep3B and Huh7. **A** A signaling time-course in Hep3B and Huh7 cells depicts mean fold changes in phospho-protein signaling in response to 1uM 17AAG relative to the vehicle only (0.1%MetOH) control. **B** The integral (discussed in methods) from 0–4hrs of 17AAG induced signaling shows the large cumulative difference in early signaling between Huh7 and Hep3B cells.

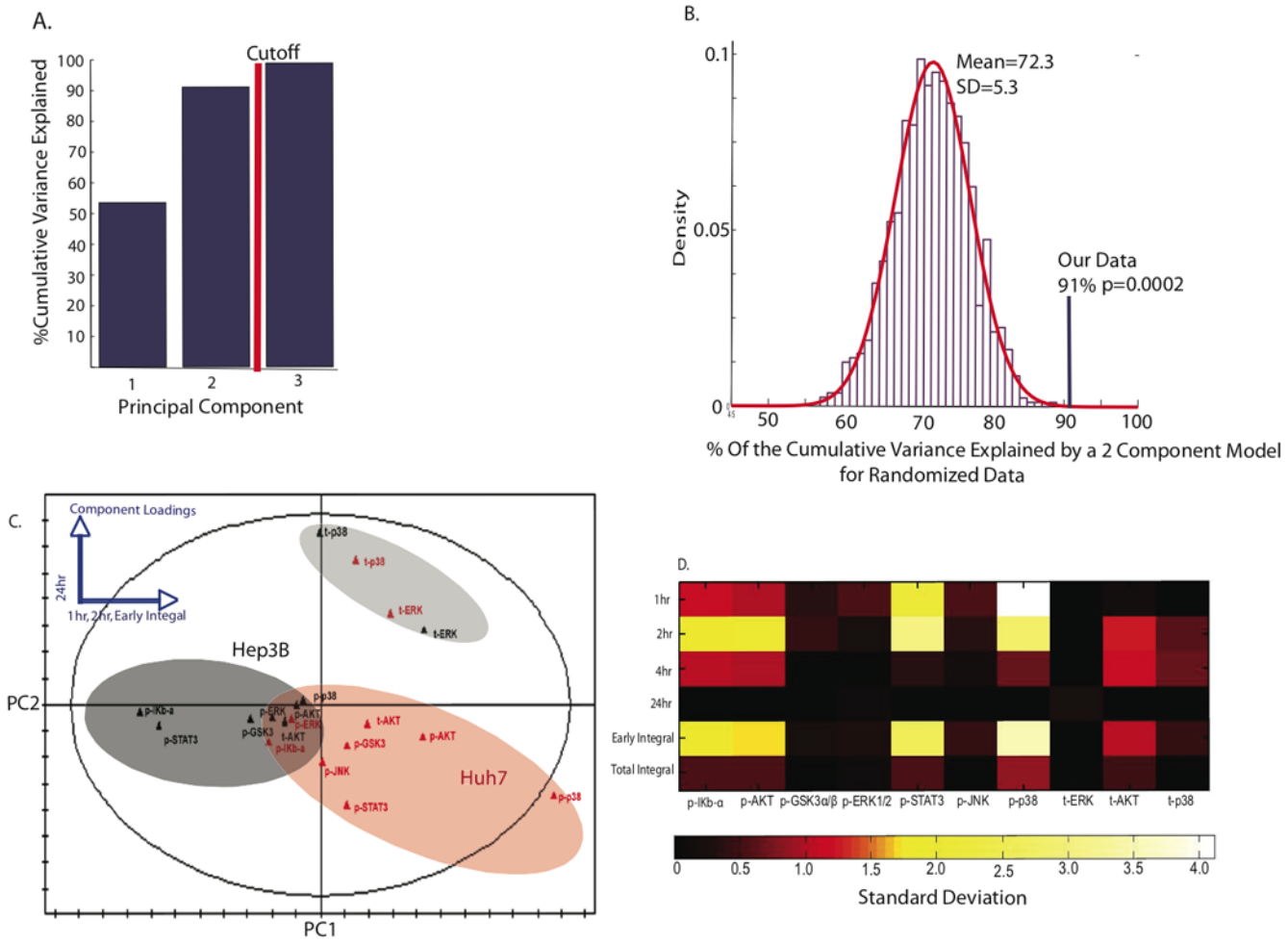

Figure 3.

A Principal Components Analysis reduces data complexity and provides testable hypotheses. **A** A bar graph depicts the percent of the total variance captured by a model consisting of 1,2,or 3 principal components. There is a marginal increase in the benefit of including principal component 3, indicating an obvious cutoff criterion. **B** The % of total variance explained by two component models that are built upon 1000 perturbed data matrices (see methods). A histogram plots the data from the empirical 1000 matrix sampling. A normal distribution was fit to the histogram data and our model fit was calculated to have a highly significant p-value of 0.0002. **C** A principal components analysis yielded a two component model that accurately explains 91% of the cumulative variance. Principal component 1 strongly captures variation at early time points, and in the 0–4hrs integral metric. Principal component 2 captures variation at 24hrs. These results from the loadings plot are summarized in the upper right-hand corner of the plot. The ellipse represents Hotelling's outlier criteria at a 95% confidence level. The original signaling measurements are plotted in the principal components space. Principal component 1 visually appears to capture cell line variation. The colored ellipses are simply a visualization tool used to bring the readers attention to the distinct clusters in the scores plot. **D** Contributions vectors describe how signals vary in principal components space, and, are derived computationally, by measuring the latent variable distance in terms of the Euclidean distance of the measured variables between Huh7 and Hep3B for a given signal, then comparing that distance to an average distance of all the distances between the cell lines (in units of standard deviation). This plot asks the question of how distinct are two signals between Huh7

and Hep3B cells relative to the average distance between lines. Quantitatively, D. affirms qualitative observations made in C.

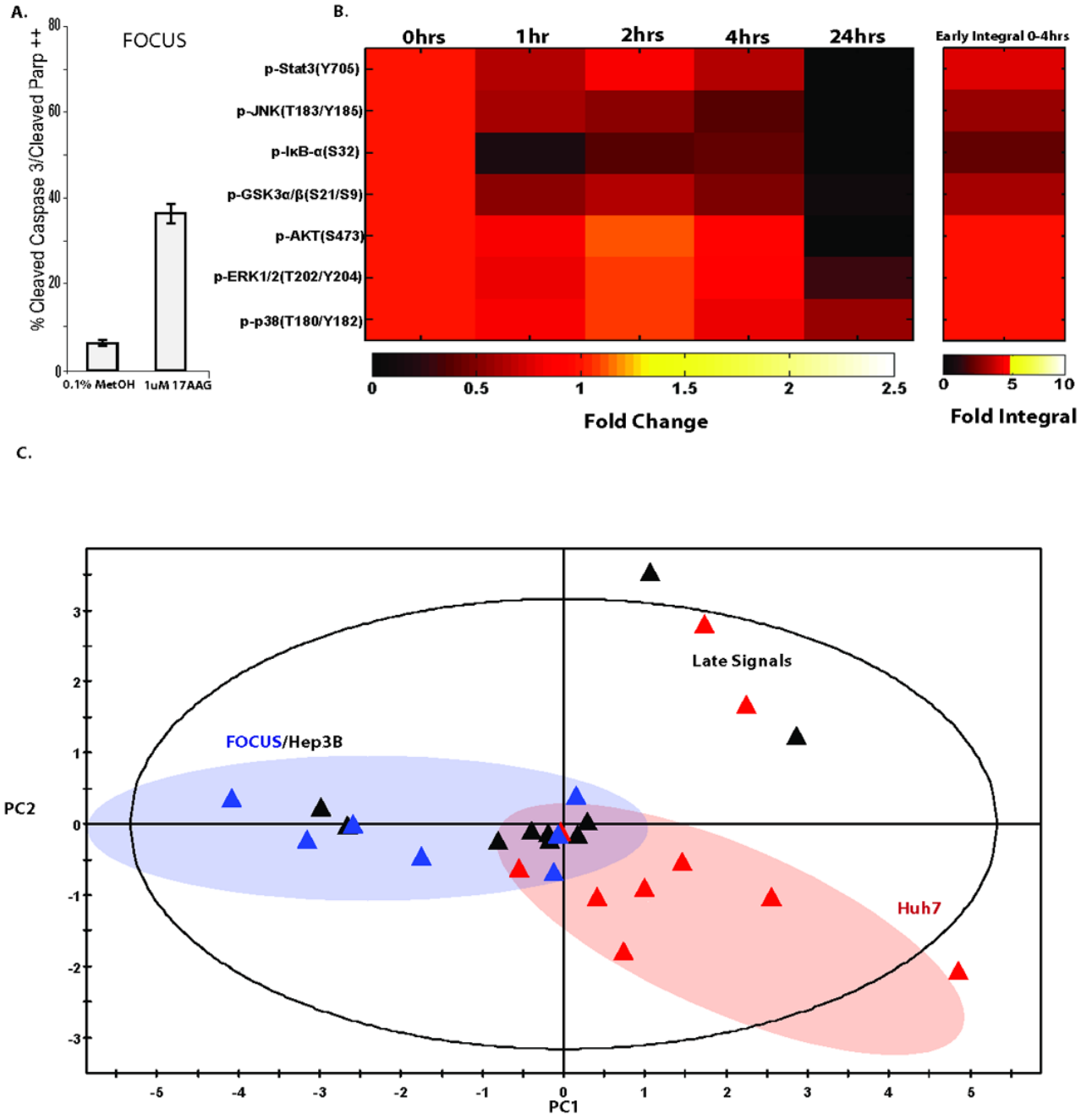

Figure 4.

Adding signaling data from another HCC cell line (FOCUS) to the principal components analysis correctly clusters FOCUS cells with sensitive Hep3B cells. **A** The mean of triplicate measurements of the percent of double positive FOCUS cells in response to 1uM 17AAG at 48 hrs. The gating strategy was the same as in 1A. **B** A signaling time-course of FOCUS cells in response to 1uM 17AAG. Time-point measurements are represented as mean signaling fold change relative to vehicle only controls. **C** A principal components scores plot, as in figure 3 correctly classifies FOCUS cell phosphoprotein signaling measurements as homologous to 17AAG sensitive Hep3b cells in the 2-component model.

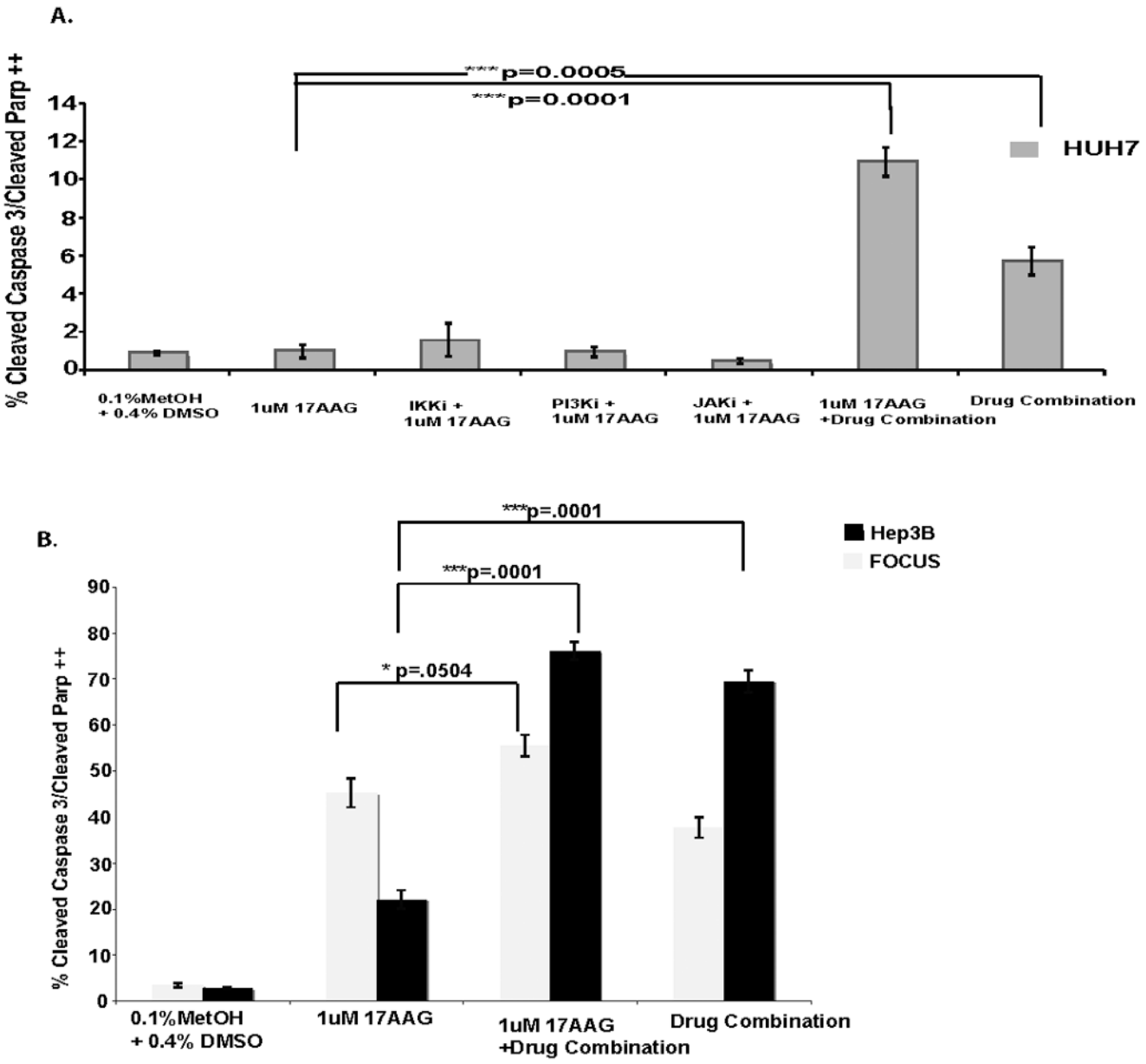

Figure 5.

Where inhibition of singular nodes fails, pre-treatment with a combination therapy sensitizes Huh7 cells to 17AAG, and works as well or better than 17AAG in all cell lines tested. **A** Double positive populations of Huh7 cells (mean of triplicate+/−SEM as gated in 1A) in response to different treatments at 48hours. The IKK inhibitor is BMS-345541 and was used at 15uM, the PI3K inhibitor is PI103 and was used at 5μM, the JAK inhibitor is Calbiochem JAK inhibitor 1: Pyridone 6, and was used at 3μM. The P-values were obtained by a T-test **B** The double-positive populations for the listed treatments of Hep3B and FOCUS cells (mean of triplicates +/−SEM) at 48 hours. The P-values were obtained by a T-test. The drug combination is the same as in A.

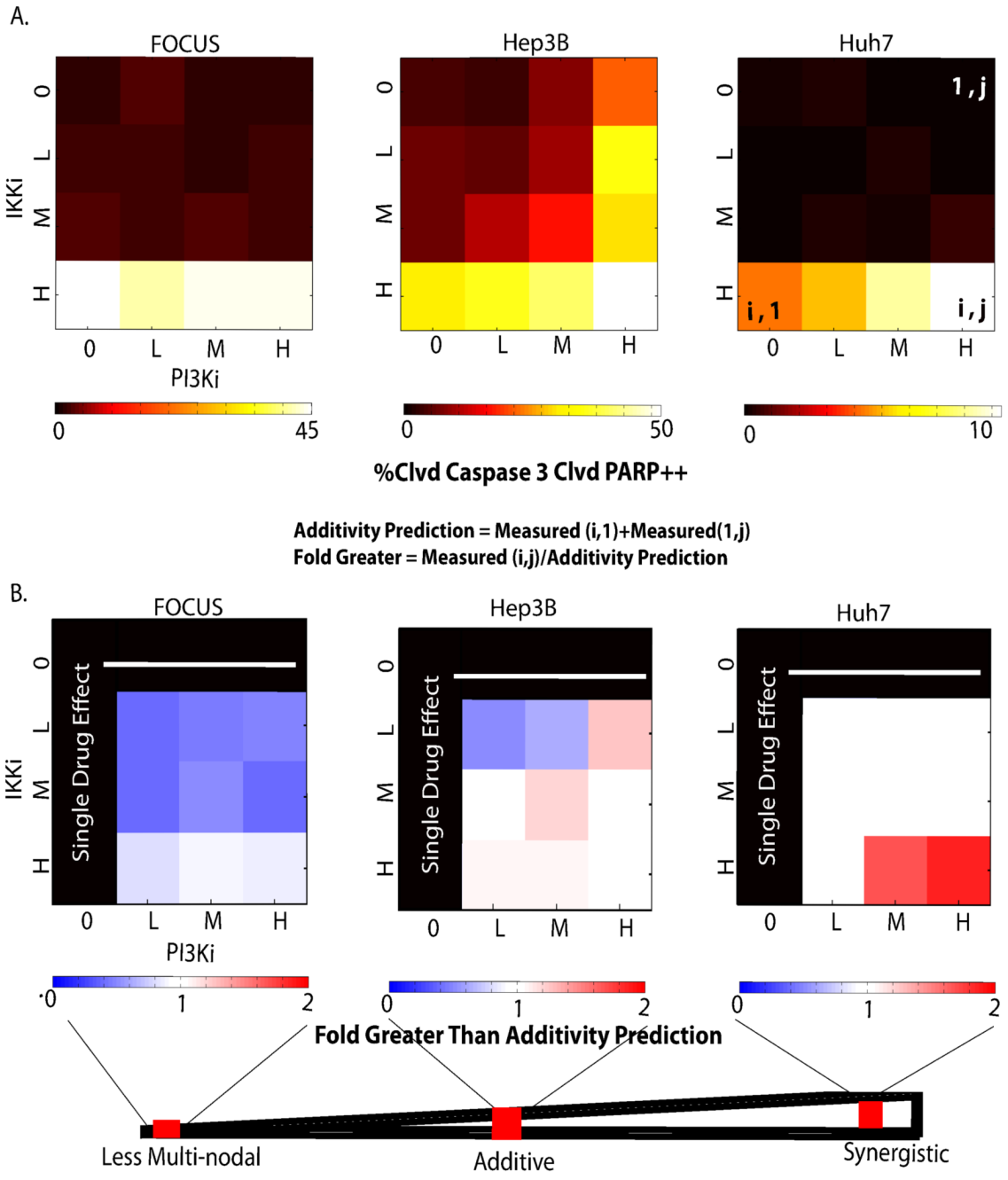

Figure 6.

Focus, Huh7 and Hep3B cells exhibit different amounts of multi-node effects in a JAK inhibitor background. **A** A matrix of the mean of duplicate measurements of the percent of double positive cells in response to varying concentrations of I-kappa-kinase inhibitor (IKKi) and PI3kinase inhibitor (PI3Ki) in a JAK (3μM) inhibitor background. The compounds are the same as in figure 4. Concentrations are as follows: (IKKi, H=20μM, M=6.66μM, L=2.22μM), (PI3Ki, H=5μM, M=1.66μM, L=0.55μM). **B** The synergy plots display the fold deviation from predictions based on the assumption of additivity. Briefly, additivity predictions for any double-drugged entry (i,j) were calculated by adding the ith row of the first column (i.e. the singular IKK effect at that concentration) to the first row, jth column (i.e. the singular PI3k

effect at that concentration). Then the measured value at the double-drugged entry (i,j) was divided by the additivity prediction. This created a metric that describes synergy versus additivity.